J|A|C|S ARTICLES

Published on Web 09/10/2010

Latent Porosity in Potassium Dodecafluoro-*closo*-dodecaborate(2−). Structures and Rapid Room Temperature Interconversions of Crystalline $K_2B_{12}F_{12}$, $K_2(H_2O)_2B_{12}F_{12}$, and $K_2(H_2O)_4B_{12}F_{12}$ in the Presence of Water Vapor

Dmitry V. Peryshkov,[†] Alexey A. Popov,[‡] and Steven H. Strauss*,[†]

Department of Chemistry, Colorado State University, Fort Collins, Colorado 80523, and Department of Electrochemistry and Conducting Polymers, Leibniz Institute for Solid State and Materials Research, Dresden D01069, Germany

Received June 23, 2010; E-mail: steven.strauss@colostate.edu

Abstract: Structures of $K_2(H_2O)_2B_{12}F_{12}$ and $K_2(H_2O)_4B_{12}F_{12}$ were determined by X-ray diffraction. They contain $[K(\mu\text{-}H_2O)_2K]^{2+}$ and $[(H_2O)K(\mu\text{-}H_2O)_2K(H_2O)]^{2+}$ dimers, respectively, which interact with superweak $B_{12}F_{12}^{2-}$ anions via multiple K···F(B) interactions and (O)H···F(B) hydrogen bonds (the dimers in $K_2(H_2O)_4B_{12}F_{12}$ are also linked by (O)H···O hydrogen bonds). DFT calculations show that both dimers are thermodynamically stabilized by the lattice of anions: the predicted ΔE values for the gas-phase dimerization of two $K(H_2O)^+$ or $K(H_2O)_2^+$ cations into $[K(\mu\text{-}H_2O)_2K]^{2+}$ or $[(H_2O)K(\mu\text{-}H_2O)_2K(H_2O)]^{2+}$ are +232 and +205 kJ mol^{-1}, respectively. The calculations also predict that ΔE for the gas-phase reaction $2\ K^+ + 2\ H_2O \rightarrow [K(\mu\text{-}H_2O)_2K]^{2+}$ is +81.0 kJ mol, whereas ΔH for the reversible reaction $K_2B_{12}F_{12\,(s)} + 2\ H_2O_{(g)} \rightarrow K_2(H_2O)_2B_{12}F_{12\,(s)}$ was found to be −111 kJ mol^{-1} by differential scanning calorimetry. The $K_2(H_2O)_{0,2,4}B_{12}F_{12}$ system is unusual in how rapidly the three crystalline phases (the $K_2B_{12}F_{12}$ structure was reported recently) are interconverted, two of them reversibly. Isothermal gravimetric and DSC measurements showed that the reaction $K_2B_{12}F_{12\,(s)} + 2\ H_2O_{(g)} \rightarrow K_2(H_2O)_2B_{12}F_{12\,(s)}$ was complete in as little as 4 min at 25 °C when the sample was exposed to a stream of He or N_2 containing 21 Torr $H_2O_{(g)}$. The endothermic reverse reaction required as little as 18 min when $K_2(H_2O)_2B_{12}F_{12}$ at 25 °C was exposed to a stream of dry He. The products of hydration and dehydration were shown to be crystalline $K_2(H_2O)_2B_{12}F_{12}$ and $K_2B_{12}F_{12}$, respectively, by PXRD, and therefore these reactions are reconstructive solid-state reactions (there is also evidence that they may be single-crystal-to-single-crystal transformations when carried out very slowly). The hydration and dehydration reaction times were both particle-size dependent and carrier-gas flow rate dependent and continued to decrease up to the maximum carrier-gas flow rate of the TGA instrument that was used, demonstrating that the hydration and dehydration reactions were limited by the rate at which $H_2O_{(g)}$ was delivered to or swept away from the microcrystal surfaces. Therefore, the rates of absorption and desorption of H_2O from unit cells at the surface of the microcrystals, and the rate of diffusion of H_2O across the moving $K_2(H_2O)_2B_{12}F_{12\,(s)}/K_2B_{12}F_{12\,(s)}$ phase boundary, are even faster than the fastest rates of change in sample mass due to hydration and dehydration that were measured. The exchange of 21 Torr $H_2O_{(g)}$ with either D_2O or $H_2{}^{18}O$ in microcrystalline $K_2(D_2O)_2B_{12}F_{12}$ or $K_2(H_2{}^{18}O)_2B_{12}F_{12}$ at 25 °C was also facile and required as little as 45 min to go to completion ($H_2O_{(g)}$ replaced both types of isotopically labeled water at the same rate for a given starting sample of $K_2B_{12}F_{12}$, demonstrating that water molecules were exchanging, not protons. Significant portions of mass (m) vs time (t) plots for the $^{1,2}H_2O_{(g)}/K_2(^{2,1}H_2O)_2B_{12}F_{12\,(s)}$ exchange reactions fit the equation $m \propto e^{-kt}$, with $10^3k = 1.9\ s^{-1}$ for one particle size distribution and $10^3k = 0.50\ s^{-1}$ for another. Finally, $K_2(H_2O)_2B_{12}F_{12}$ was not transformed into $K_2(H_2O)_4B_{12}F_{12}$ after prolonged exposure to 21 Torr $H_2O_{(g)}$ at 25 °C, 37 Torr $H_2O_{(g)}$ at 35 °C, or 55 Torr $H_2O_{(g)}$ at 45 °C.

Introduction

The rapid and reversible absorption/desorption of small molecules by rigid[1−5] or flexible (breatheable)[6−9] microporous solids is a historically important[10−12] as well as current area of fundamental and applied research. In addition to technological applications, rapid and reversible absorption reactions involving crystalline materials can serve as model systems for studying

[†] Colorado State University.
[‡] Leibniz Institute for Solid State and Materials Research.

(1) Marion, S.; Meyer, H.-W.; Carpenter, M.; Norby, T. *Am. Mineral.* **2001**, *86*, 1166–1169.
(2) Lee, Y.; Kim, S. J.; Bull, I.; Celestian, A. J.; Parise, J. B.; Kao, C.-C.; Vogt, T. *J. Am. Chem. Soc.* **2007**, *129*, 13744–13748.
(3) Xu, M.; Harris, K. D. M.; Thomas, J. M. *J. Am. Chem. Soc.* **2008**, *130*, 5880–5882.
(4) O'Hare, B.; Grutzeck, M. W.; Kim, S. H.; Asay, D. B.; Benesi, A. J. *J. Mag. Reson.* **2008**, *195*, 85–102.
(5) Wang, H.-W.; Bish, D. L. *Eur. J. Mineral.* **2010**, *22*, 271–284.

 10.1021/ja105522d

the mechanisms of solid-state reactions, whether or not those reactions involve single-crystal-to-single-crystal transformations.[1−4,13−21] The difficulties of combining the frequently incompatible features of thermal stability, porosity, reversible dynamic motion, and crystallinity in solids has been discussed recently.[21]

We are investigating a new concept in the creation of microporosity, combining the large, highly-symmetric, rigid, and robust superweak[22−25] anion $B_{12}F_{12}^{2-}$[26,27] with metal ions that have few or no ancillary ligands. This has the potential to create real or virtual (i.e., latent) coordinative unsaturation[28−30] at a metal center in a crystalline material, enabling small molecules L to displace some or all of the weak, nondirectional M···F(B) bonds, and in so doing create their own micropores as needed. In principle, the high symmetry and superweak nature of the $B_{12}F_{12}^{2-}$ anion might render lattice-expanding equilibria such as $M_xB_{12}F_{12} + nx\ L \rightleftharpoons [ML_n]_xB_{12}F_{12}$ rapid enough, even at mild temperatures, to be useful in a variety of applications for which microporous materials are typically used, including catalysis, separations, absorbents, membranes, sensors, and devices that conduct ions or electrons.[9−12,31−35]

We herein report that $K_2B_{12}F_{12}$, the large-scale synthesis[36] and solid-state structure[37] of which were reported recently, can be recrystallized from water to yield two different hydrates, $K_2(H_2O)_2B_{12}F_{12}$ and $K_2(H_2O)_4B_{12}F_{12}$, the structures of which have been determined by single-crystal X-ray diffraction. The three compounds $K_2(H_2O)_nB_{12}F_{12}$ ($n = 0, 2, 4$) are related by a series of solid-state hydration and/or dehydration reactions, the rates of which have been determined under certain sets of conditions in an initial kinetic study. These are remarkably rapid transformations. The reversible dehydration of crystalline $K_2(H_2O)_2B_{12}F_{12}$ to crystalline $K_2B_{12}F_{12}$ in a stream of dry helium was fast at 25(1) °C ($\Delta H = 111(1)$ kJ mol^{-1} by DSC; >98% complete in as little as 18 min depending on the size of the sample particles) and the exothermic rehydration in a stream of water-saturated helium was even faster (in as little as 4 min), and these reaction times were limited by the carrier-gas flow rate. Furthermore, the exchange of H_2O in the vapor phase with either D_2O or $H_2{}^{18}O$ in $K_2(D_2O)_2B_{12}F_{12}$ or $K_2(H_2{}^{18}O)_2B_{12}F_{12}$ at 25.0(5) °C was also facile and required as little as 45 min to go to completion. These results demonstrate that permanent porosity is not required for rapid and reversible gas absorption and for rapid gas diffusion in crystalline solids at ordinary temperatures. It can be achieved in an all-inorganic system with the large, symmetric, rigid, and robust superweak anion $B_{12}F_{12}^{2-}$.

Experimental Section

The anhydrous salt $K_2B_{12}F_{12}$ was prepared as previously described.[36] Distilled water was passed through a Barnstead Nanopure deionizer; the deionized distilled water had a resistivity of at least 18 MΩ. Samples of the water isotopomers D_2O (99.9% D) and $H_2{}^{18}O$ (97% ^{18}O) were obtained from Cambridge Isotope Laboratories, Inc., and used as received. Copper(II) sulfate pentahydrate (Fisher) was used as received. Single crystals of $K_2(H_2O)_2B_{12}F_{12}$ and $K_2(H_2O)_4B_{12}F_{12}$ were grown by slow evaporation of water from a saturated aqueous solution of $K_2B_{12}F_{12}$ at 23(1) °C or cooling a saturated aqueous solution of $K_2B_{12}F_{12}$ to 0 °C, respectively.

The vapor pressures of rigorously degassed H_2O and D_2O at 23.0(1) °C were determined to be 21.1(1) and 18.1(1) Torr, respectively, by vacuum-line tensimetry, and are the same as values reported in the literature.[38,39] Samples for isothermal thermogravimetric analysis (TGA; platinum sample pans; *ca.* 10 mg samples; 25.0(5) or 35.0(5) °C) and differential scanning calorimetry (DSC; aluminum sample pans, *ca.* 10 mg samples; 25.0(5) °C) were analyzed using TA Instruments Series-2950 instrumentation. Dry helium or helium bubbled through H_2O or D_2O at 23(1) °C (TGA) or dry nitrogen or nitrogen bubbled through H_2O or D_2O at 23(1) °C (DSC) with flow rates that varied from 60 to 100 mL min^{-1} depending on the experiment was used to maintain a constant-composition atmosphere above the samples ($P(H_2O) = 21(1)$ Torr at 23(1) °C). However, when dry carrier gas was switched to wet carrier gas (or vice versa), there was a delay of several minutes before the composition of the atmosphere in the sample chamber became constant (as monitored by the mass spectrum of the carrier gas exiting the sample chamber). X-ray powder diffraction patterns

(6) Bureekaew, S.; Shimomura, S.; Kitagawa, S. *Sci. Technol. Adv. Mater.* **2008**, *9* (12 pp), 014108.
(7) Colodrero, R. M. P.; Cabeza, A.; Olivera-Pastor, P.; Infantes-Molina, A.; Barouda, E.; Demadis, K. D.; Aranda, M. A. G. *Chem.—Eur. J.* **2009**, *15*, 6612–6619.
(8) Férey, G.; Serre, C. *Chem. Soc. Rev.* **2009**, *38*, 1380–1399.
(9) Li, J.-R.; Kuppler, R. J.; Zhou, H.-C. *Chem. Soc. Rev* **2009**, *38*, 1477–1504.
(10) Sherman, J. D. *Proc. Natl. Acad. Sci. U.S.A.* **1999**, *96*, 3471–3478.
(11) Auerbach, S. M.; Carrado, K. A.; Dutta, P. K. *Handbook of Zeolite Science and Technology*; Marcel Dekker: New York, 2003.
(12) Xu, R.; Pang, W.; Yu, J.; Huo, Q.; Chen, J. *Chemistry of Zeolites and Related Porous Materials: Synthesis and Structure*; Wiley-VCH: Weinheim, 2007.
(13) Steiner, T.; Moreira da Silva, A. M.; Teixeira-Dias, J. J. C.; Müller, J.; Saenger, W. *Angew. Chem. Int. Ed.* **1995**, *34*, 1452–1453.
(14) Kawasaki, T.; Jiang, L.; Iyoda, T.; Aradki, T.; Hashimoto, K.; Fuhishima, A. *J. Phys. Chem. B* **1998**, *102*, 1989–1993.
(15) Thallapally, P. K.; Lloyd, G. O.; Atwood, J. L.; Barbour, L. J. *Angew. Chem.* **2005**, *117*, 3916–3919.
(16) Bowers, G. M.; Bish, D. L.; Kirkpatrick, R. J. *J. Phys. Chem. C* **2008**, *112*, 6430–6438.
(17) Pfeiffer, H.; Lima, E.; Lara, V.; Velente, J. S. *Langmuir* **2009**, *26*, 4074–4079.
(18) Volkringer, C.; Loiseau, T.; Guillou, N.; Férey, G.; Haouas, M.; Taulelle, F.; Audebrand, N.; Margiolaki, I.; Popov, D.; Burghammer, M.; Riekel, C. *Cryst. Growth Des.* **2009**, *9*, 2927–2936.
(19) Mobin, S. M.; Srivastava, A. K.; Mathur, P.; Lahiri, G. K. *Inorg. Chem.* **2009**, *48*, 4652–4654.
(20) Noisong, P.; Danvirutai, C. *Ind. Eng. Chem. Res.* **2010**, *49*, 3146–3151.
(21) Chandler, B. D.; Enright, G. D.; Udachin, K. A.; Pawsey, S.; Ripmeester, J. A.; Cramb, D. T.; Shimizu, G. K. H. *Nat. Mater.* **2008**, *7*, 229–235.
(22) Lupinetti, A. J.; Strauss, S. H. *Chemtracts* **1998**, *11*, 565–595.
(23) Krossing, I.; Raabe, I. *Angew. Chem.* **2004**, 2066–2090.
(24) Strauss, S. H. *Chem. Rev.* **1993**, *93*, 927–942.
(25) Ivanova, S. M.; Nolan, B. G.; Kobayashi, Y.; Miller, S. M.; Anderson, O. P.; Strauss, S. H. *Chem.—Eur. J.* **2001**, *7*, 503–510.
(26) Solntsev, K. A.; Mebel, A. M.; Votinova, N. A.; Kuznetsov, N. T.; Charkin, O. P. *Koord. Khim.* **1992**, *18*, 340–364.
(27) Ivanov, S. V.; Miller, S. M.; Anderson, O. P.; Solntsev, K. A.; Strauss, S. H. *J. Am. Chem. Soc.* **2003**, *125*, 4694–4695.
(28) Rach, S. F.; Kühn, F. E. *Chem. Rev.* **2009**, *109*, 2061–2080.
(29) Hurlburt, P. K.; Van Seggen, D. M.; Rack, J. J.; Strauss, S. H. In *Inorganic Fluorine Chemistry Toward the 21st Century*; Thrasher, J. S., Strauss, S. H., Eds.; ACS Symposium Series 555; American Chemical Society: Washington, DC, 1994; pp 338−349.
(30) Strauss, S. H. *Chemtracts: Inorg. Chem.* **1994**, *6*, 1–13.
(31) Lee, J.; Farha, O. K.; Roberts, J.; Scheidt, K. A.; Nguyen, S.; Hupp, J. T. *Chem. Soc. Rev.* **2009**, *38*, 1450–1459.
(32) Czaja, A. U.; Trukhan, N.; Müller, U. *Chem. Soc. Rev.* **2009**, *38*, 1284–1293.
(33) Hurd, J. A.; Vaidhyanathan, R.; Thangadurai, V.; Ratcliffe, C. I.; Moudrakovski, I. L.; Shimizu, G. K. H. *Nat. Chem.* **2009**, *1*, 705–710.
(34) Pérez-Ramírez, J.; Christensen, C. H.; Egeblad, K.; Christensen, C. H.; Groen, J. C. *Chem. Soc. Rev.* **2008**, *37*, 2530–2542.
(35) Stöcker, M. *Microporous Mesoporous Mater.* **2005**, *82*, 257–292.
(36) Peryshkov, D. V.; Popov, A. A.; Strauss, S. H. *J. Am. Chem. Soc.* **2009**, *131*, 18393–18403.
(37) Peryshkov, D. V.; Strauss, S. H. *J. Fluorine Chem.* **2010**, in press (doi:10.1016-/j.jfluchem.2010.06.015).
(38) Besley, L.; Bottomley, G. A. *J. Chem. Thermodyn.* **1973**, *5*, 397–410.
(39) Jákli, G.; Van Hook, W. A. *J. Chem. Eng. Data* **1981**, *26*, 243–245.

Table 1. Crystallographic and Data-Collection Parameters

compound	$K_2(H_2O)_2B_{12}F_{12}$	$K_2(H_2O)_4B_{12}F_{12}$
empirical formula	$B_{12}F_{12}H_4K_2O_2$	$B_{12}F_{12}H_8K_2O_4$
formula weight	471.95	507.98
habit, color	prism, colorless	prism, colorless
space group	$P2_1/c$	$P\bar{1}$
a (Å)	7.2955(2)	8.3988(3)
b (Å)	11.2522(3)	8.5982(4)
c (Å)	9.2260(2)	12.7454(5)
α (deg)	90	98.830(2)
β (deg)	103.730(1)	102.056(2)
γ (deg)	90	104.958(2)
V (Å^3)	735.80(3)	848.39(6)
Z	2	2
T (K)	110(2)	110(2)
ρ_{calc} (g cm^{-3})	2.1302(1)	1.9886(1)
$R(F)$ $(I > 2\sigma(I))^a$	0.0198	0.0204
$wR(F^2)$ [all data]^a	0.0579	0.0582
min., max. e$^-$ dens. (e Å^{-3})	−0.449, 0.281	−0.412, 0.277

^{a} $R(F) = \Sigma||F_o| - |F_c||/\Sigma|F_o|$; $wR(F^2) = (\Sigma[w(F_o^2 - F_c^2)^2]/\Sigma[w(F_o^2)^2])^{1/2}$.

were recorded using a Scintag X2 X-ray diffractometer (Cu Kα radiation) at 25(1) °C with a step size of 0.02° and a scan rate of 1.67° min^{-1}. FTIR spectra were recorded with a Nicolet Magna-760 FTIR spectrometer operating at 2 cm^{-1} resolution using a special IR cell of local design.[40] The "D_2O sample" was not allowed to undergo complete isotopomer exchange, so the sample was $K_2(H_2O)_x(HDO)_y(D_2O)_zB_{12}F_{12}$ where $x + y + z = 2$. Scanning electron microscopy was performed on a finely ground sample of anhydrous $K_2B_{12}F_{12}$ using a JSM-6500F field emission system (operating voltage =15 kV). A 5 nm layer of gold was sputtered onto the surface of the sample to make it conductive.

X-ray diffraction data from single crystals of $K_2(H_2O)_2B_{12}F_{12}$ and $K_2(H_2O)_4B_{12}F_{12}$ were collected with a Bruker Kappa APEX II CCD diffractometer at 110(2) K employing Mo Kα radiation (graphite monochromator). Unit cell parameters, listed in Table 1, were obtained from least-squares fits to the angular coordinates of all reflections, and intensities were integrated from a series of frames (ω and φ rotation) covering more than a hemisphere of reciprocal space. Absorption and other corrections were applied using SADABS.[41] The structures were solved using direct methods and refined (on F^2 using all data) by a full-matrix, weighted least-squares process. Standard Bruker control and integration software (APEX II) was employed,[42] and Bruker SHELXTL software was used for structure solution, refinement, and molecular graphics.[43] In both structures the displacement parameters of H atoms of the H_2O molecules were constrained as $U_{eq}(H) = 1.5U_{eq}(O)$ and O−H bond distances were restrained to be similar within each molecule.

DFT Calculations. All DFT calculations were performed using the ORCA code.[44] The B2-PLYP-D functional[45−49] and def2-QZVPP basis set[50] augmented with diffuse functions from the aug-cc-pVTZ basis set[51] for oxygen and hydrogen atoms were employed for all calculations. The B2-PLYP-D double hybrid density functional includes a semiempirical mixture of DFT and MP2 correlation energies[47,49] as well as semiempirical correction to account for dispersion forces.[48] Symmetry restrictions were not used in the course of the optimization.

Results and Discussion

I. Structures of $K_2(H_2O)_2B_{12}F_{12}$ and $K_2(H_2O)_4B_{12}F_{12}$. A. Anions and Cations. Selected interatomic distances and angles are listed in Table 2, which also includes distances and angles for $K_2B_{12}F_{12}$[37] for comparison. There is a single $B_{12}F_{12}^{2-}$ anion in the structure of the dihydrate and two distinct $B_{12}F_{12}^{2-}$ anions in the structure of the tetrahydrate. All three anions sit on inversion centers in their respective lattices, and therefore each exhibits 15 unique B−B bonds and 6 unique B−F bonds. As expected, all three are nearly icosahedral and are otherwise unremarkable. The structure of $K_2(H_2O)_2B_{12}F_{12}$ is the most precise structure of any compound containing a $B_{12}X_{12}^{2-}$ dianion (the standard errors on individual B−B and B−F bonds are 0.0009 and 0.0007 Å, respectively). Plots of the unique B−B and B−F distances for the $B_{12}F_{12}^{2-}$ anions in both structures (also showing the DFT-predicted distances for the isolated anion) are shown in Figure S-1 (Supporting Information (S.I.)). All of the F atoms of the $B_{12}F_{12}^{2-}$ anions are either bonded to K^+ ions (i.e., K···F < 3.3 Å) or are hydrogen-bonded to H atoms belonging to the water molecules (i.e., F···H < 2.2 Å) except for F3 in $K_2(H_2O)_4B_{12}F_{12}$, as shown in Figures 1 and 2. The KO_2F_6 coordination geometry in $K_2(H_2O)_2B_{12}F_{12}$ is a distorted square antiprism, as shown in Figure S-2. The KO_3F_5 coordination geometries in $K_2(H_2O)_4B_{12}F_{12}$ are a bicapped trigonal prism for K1 and a distorted square antiprism for K2, as shown in Figures S-3 and S-4. The K^+ bond-valence sums[52] are 1.01 in $K_2(H_2O)_2B_{12}F_{12}$ and 1.13 and 1.07 for K1 and K2, respectively, in $K_2(H_2O)_4B_{12}F_{12}$.

B. Lattices. The array of $B_{12}F_{12}^{2-}$ anions in the simple salt $K_2B_{12}F_{12}$ was recently shown to be approximately hexagonal close-packed, with K^+ ions in all of the O_h holes and in all of the D_{3h} trigonal holes that lie between pairs of T_d holes (this structure (the Ni_2In structure) is very unusual for an A_2X salt under ordinary conditions; note that the set of D_{3h} trigonal holes between pairs of O_h holes are empty in this structure).[37] The 12 nearest-neighbor distances between the B_{12} centroids (i.e., the cent···cent distances) were found to be 8.207 and 8.236 Å within the pseudo-close-packed layers and 7.204, 7.471, and 7.517 Å between the layers. The arrays of anions in the two hydrates are best described as distorted variations of the CsCl structure with two K^+ ions occupying the parallelepiped (i.e., pseudorhombohedral) voids between the $B_{12}F_{12}^{2-}$ anions, as shown in Figure 3, which also shows a similar view of the $K_2B_{12}F_{12}$ lattice for comparison. The parallelepiped in $K_2(H_2O)_2B_{12}F_{12}$ is the closest to being a cube: the cent···cent distances only vary by 0.3% (7.276 and 7.295 Å), but the cubes are tilted so that the acute cent···cent···cent angles are 78.7° and 81.3° instead of 90° (for comparison, the corresponding angles are 71.7°, 75.0°, and 75.3° in $K_2(H_2O)_4B_{12}F_{12}$ and 54.3°, 56.4°, and 60.1° in nearly close-packed $K_2B_{12}F_{12}$).

The drawings in Figure 3 and the distances and angles listed in Table 1 show that the dehydration/rehydration reactions $K_2(H_2O)_4B_{12}F_{12} \rightarrow K_2(H_2O)_2B_{12}F_{12} \rightleftharpoons K_2B_{12}F_{12}$, the kinetics and

(40) Rack, J. J.; Polyakov, O. G.; Gaudinski, C. M.; Hammel, J. W.; Kasperbauer, P.; Hochheimer, H. D.; Strauss, S. H. *Appl. Spectrosc.* **1998**, *52*, 1035–1038.
(41) Sheldrick, G. M. *SADABS, v. 2.10−A program for area detector absorption corrections*; Bruker AXS: Madison, WI, 2003.
(42) Sheldrick, G. M. *APEX2, v. 2.0-2*; Bruker AXS: Madison, WI, 2006.
(43) Sheldrick, G. M. *SHELXTL, v. 6.12 UNIX*; Bruker AXS: Madison, WI, 2001.
(44) Neese, F. *ORCA, an ab initio, density functional and semiempirical program package, Version 2.7-00*; Institute for Physical and Theoretical Chemistry: Bonn, 2009.
(45) Becke, A. D. *Phys. Rev. A* **1998**, *38*, 3098–3100.
(46) Lee, C.; Yang, W.; Parr, R. G. *Phys. Rev. B* **1988**, *37*, 785–789.
(47) Grimme, S. *J. Chem. Phys.* **2006**, *124*, 034108.
(48) Grimme, S. *J. Comput. Chem.* **2006**, *27*, 1787–1799.
(49) Neese, F.; Schwabe, T.; Grimme, S. *J. Chem. Phys.* **2007**, *126*, 124115.
(50) Weigend, F.; Ahlrichs, R. *Phys. Chem. Chem. Phys.* **2005**, *7*, 3297–3305.
(51) Kendall, R. A.; Dunning, J., T. H.; Harrison, R. J. *J. Chem. Phys.* **1992**, *96*, 6796.
(52) Brown, I. D. *Chem. Rev.* **2009**, *109*, 6858–6919, and references therein.

Table 2. Selected Interatomic Distances (Å) and Angles (deg)[a]

parameter	$K_2B_{12}F_{12}$[b]	$K_2(H_2O)_2B_{12}F_{12}$	$K_2(H_2O)_4B_{12}F_{12}$
K−F(B)	2.651(2)−3.405(2) (K1); 2.615(2)−3.324(2) (K2)	2.5984(4)−3.1593(5)	2.6501(6)−3.2843(6) (K1); 2.7069(8)−3.2843(7) (K2)
K−F−B	92.8(2)−159.4(2) (K1); 116.9(2)−165.5(2) (K2)	102.16(3)−163.34(4)	110.25(5)−155.16(5) (K1); 110.15(5)−150.57(5) (K2)
K−O	—	2.7698(6), 2.7716(6)	2.6685(7), 2.8126(8), 2.8306(8) (K1); 2.7070(8), 2.7469(9), 2.7703(9) (K2)
K−O−K′	—	100.26(2)	103.47(2) (K1); 98.42(3) (K2)
O−K−O′	—	79.74(2)	76.53(2)−138.92(3) (K1); 81.58(3)−140.94(3) (K2)
F···H(O)	—	2.116(14); 2.180(14)	2.14(1); 2.16(1)
O···O	—	—	2.888(1); 2.874(1)
O···H(O)	—	—	2.07(2); 2.10(2)
O···H···O	—	—	173.4(2); 174.0(2)
Σ(K−F bond valences)	1.17, 0.70	0.65	0.55 (K1); 0.45 (K2)
Σ(K−O bond valences)	—	0.35	0.54 (K1); 0.58 (K2)
Σ(all K bond valences)	1.17, 0.70	1.00	1.09 (K1); 1.03 (K2)
cent···cent	7.204−8.236 (12 distances)	7.276 × 4, 7.295 × 2	6.915 × 2, 8.399 × 2, 8.598 × 2
K···K′	5.421(1); 5.543(1); 5.629(1)	4.2529(3)	4.3188(4) (K1); 4.1293(5) (K2); 5.2470(5) (K1···K2)
B−F	1.378(3)−1.392(3)	1.3791(7)−1.3875(7)	1.378(1)−1.391(1)
B−B	1.767(4)−1.805(5)	1.7774(9)−1.8059(8)	1.781(1)−1.808(1)

[a] All data from this work unless otherwise noted; cent = B_{12} centroid. [b] From ref 37.

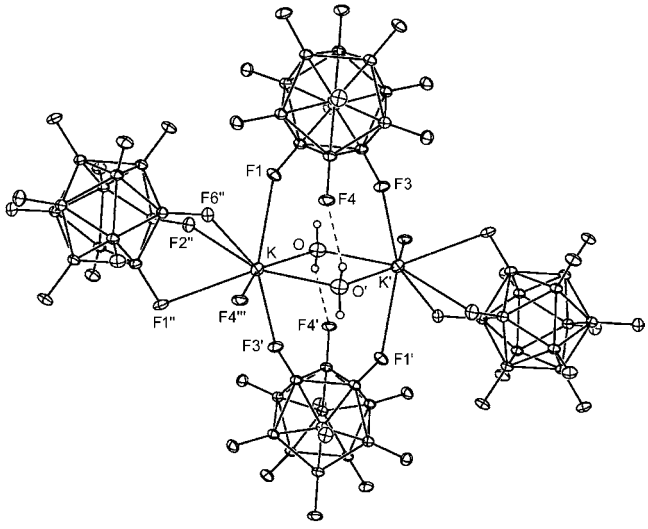

Figure 1. Structure of $K_2(H_2O)_2B_{12}F_{12}$ (50% probability ellipsoids except for H atoms). For clarity, only four of the eight $B_{12}F_{12}^{2-}$ anions that form a pseudocubic array around the $K_2(H_2O)_2^{2+}$ dimer are shown. Selected interatomic distances (Å) and angles (deg): K−O, 2.7698(6); K−O′, 2.7716(6); K−F1, 2.8251(4); K−F1″, 3.0368(4); K−F2″, 2.7790(4); K−F3′, 2.5984(4); K−F4‴, 3.1593(4); K−F6″, 2.7423(4); F4···H1′, 2.17(1); F4···H1′−O′, 154(1); K···K′, 4.2529(3) (not shown: F5⁗···H2, 2.12(1); F5⁗···H2−O, 165(1)).

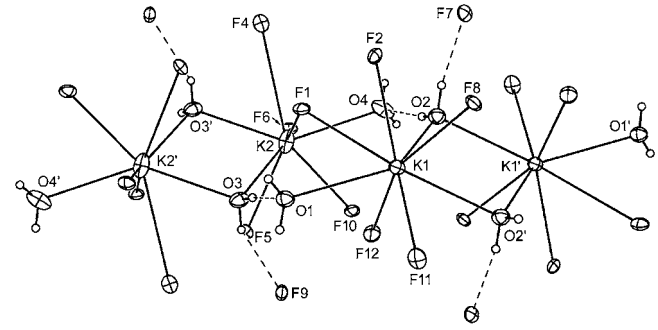

Figure 2. Structure of $K_2(H_2O)_4B_{12}F_{12}$ (50% probability ellipsoids except for H atoms). Boron atoms have been omitted for clarity. Selected interatomic distances (Å) and angles (deg): K1−O1, 2.8126(8); K1−O2, 2.6685(7); K1−O2′, 2.8306(8); K1−F1, 3.2843(6); K1−F2, 2.7698(6); K1−F8, 2.8432(6); K1−F11, 2.6655(6); K1−F12, 2.6500(6); K2−O3, 2.7469(9); K2−O3′, 2.7070(8); K2−O4, 2.7703(9); K2−F1, 2.7714(6); K2−F4, 3.2803(7); K2−F5, 3.0434(6); K2−F6, 2.7398(6); K2−F10, 2.7108(6); O1···O3, 2.888(1); O1···H3, 2.10(1); O1···H3−O3, 174.0(2); O2···O4, 2.874(1); O4···H2, 2.07(1); O4···H2−O2, 173.4(2); F7···H2′, 2.135(15); F7···H2′···O2, 158.0(16); F9···H3′, 2.156(16), F9···H3′···O3, 151.6(15); K1···K1′, 4.3188(4); K1···K2, 5.2470(4); K2···K2′, 4.1293(5).

thermodynamics of which will be discussed in the second part of this paper, can occur with relatively minor structural rearrangements involving the distances and angles between the large weakly coordinating $B_{12}F_{12}^{2-}$ anions and between the K^+ cations. The average cent···cent distances for the rhombs shown in Figure 3 are 7.987, 7.282, and 7.971 Å for $K_2B_{12}F_{12}$, $K_2(H_2O)_2B_{12}F_{12}$, and $K_2(H_2O)_4B_{12}F_{12}$, respectively, and the formula unit volumes are 332.0(2), 367.90(3), and 424.20(6) Å^3, respectively. Note, however, that the average of the 12 cent···cent distances for each B_{12} centroid in nearly close-packed $K_2B_{12}F_{12}$ is 7.812 Å, so the centroids in this compound are, on average, closer together than the rhomb in Figure 3 depicts. Note also that the B_{12} centroids are significantly closer together, on average, in $K_2(H_2O)_2B_{12}F_{12}$ than in nearly close-packed $K_2B_{12}F_{12}$ is (7.282 vs. 7.812 Å, respectively) even though the formula unit volume for the dihydrate is 10.8% larger than that for the anhydrous salt $K_2B_{12}F_{12}$.

The K1···K2 distances shown in the rhomb in Figure 3 for $K_2B_{12}F_{12}$ are 5.543(1) Å, just longer than the K1···K2 distance in $K_2(H_2O)_4B_{12}F_{12}$, which is 5.2470(4) Å. (There are also 5.421(1) Å K1···K2 distances in $K_2B_{12}F_{12}$.) The K···K′ distance in $K_2(H_2O)_2B_{12}F_{12}$ is 4.2529(3) Å and the K1···K1 and K2···K2 distances in $K_2(H_2O)_4B_{12}F_{12}$ are 4.3188(4) and 4.1293(5) Å, respectively, ca. 30% shorter than 5.5 Å. (As points of reference, the K···K distances in KF[53] and K_2O[54] are 3.795(2) and 3.218 Å, respectively; the packing of B_{12} centriods and $[K_2(H_2O)_4]^{2+}$ dimers in $K_2(H_2O)_4B_{12}F_{12}$ is shown in Figure S-5.) Therefore, as $K_2B_{12}F_{12}$ is transformed into $K_2(H_2O)_2B_{12}F_{12}$ in the presence of water vapor (see below), the weakly coordinating anions shift their positions in the lattice and pairs

(53) Finch, G. J.; Fordham, S. *Proc. Phys. Soc.* **1936**, *48*, 85–94.
(54) Zintl, E.; Harder, A.; Dauth, B. *Z. Elektrochem. Angew. Phys. Chem.* **1934**, *40*, 588–593.

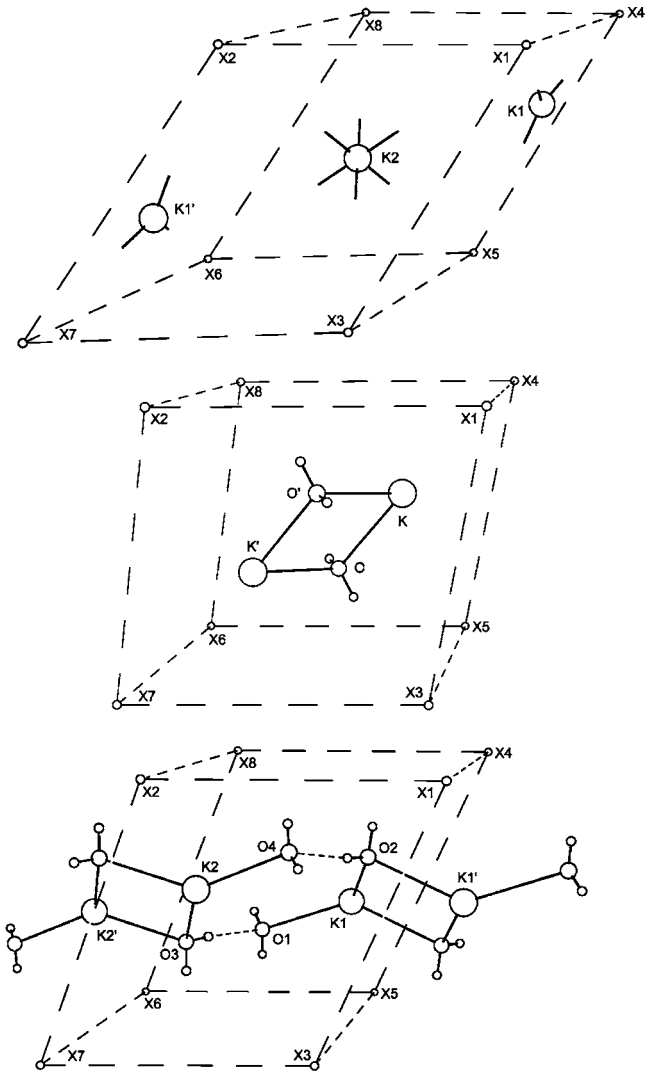

Figure 3. B_{12} centroid parallelepipeds (X1−X8) and $K_2(H_2O)_n^{2+}$ dimers in $K_2B_{12}F_{12}$ (top), $K_2(H_2O)_2B_{12}F_{12}$ (middle), and $K_2(H_2O)_4B_{12}F_{12}$ (bottom). The X1···X2, X1···X3, and X1···X4 distances (Å) are 7.517, 8.236, and 8.207 in $K_2B_{12}F_{12}$; 7.276, 7.295, and 7.276 in $K_2(H_2O)_2B_{12}F_{12}$; and 6.915, 8.598, and 8.399 in $K_2(H_2O)_4B_{12}F_{12}$. Note that the X1···X8 and X3···X6 distances in $K_2B_{12}F_{12}$ are 7.204 Å (the B_{12} centroids are approximately hexagonal close-packed in this structure). The small vectors radiating from the K^+ ions in $K_2B_{12}F_{12}$ point at the closest set of B_{12} centroids (K1 and K1′ are in trigonal holes in the close-packed layers and K2 is in an O_h hole).

of K^+ ions move from ca. 5.5 Å apart to ca. 4.2 Å apart. In both cases, the pairs of K^+ ions share pairs of $B_{12}F_{12}^{2-}$ anions, as shown in Figures 1, 4, and 5. The direct comparison in Figure 5 shows that relatively small motions of pairs of bridging anions are involved in the the solid-state transformation $K_2B_{12}F_{12\,(s)} + 2\ H_2O_{(g)} \rightleftharpoons K_2(H_2O)_2B_{12}F_{12\,(s)}$.

C. $K_2(H_2O)_2^{2+}$ and $K_2(H_2O)_4^{2+}$ Dimers. Table 3 lists relevant DFT and experimental results. We validated our DFT methodology by comparing results for the gas-phase monocations $K(H_2O)^+$ and $K(H_2O)_2^+$ with recent counterpoise-corrected DFT results[55] and with the classic experimental work of Kebarle and coworkers.[56,57] (We performed calculations using both TZVPP and QZVPP basis sets with no significant change in the results,

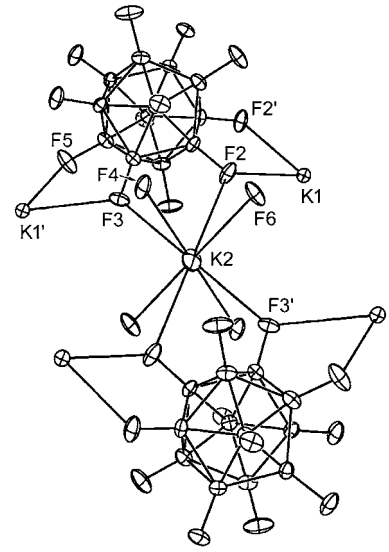

Figure 4. Part of the structure of $K_2B_{12}F_{12}$ (50% probability ellipsoids), showing the bridges formed between the K1 and K2 cations by the $B_{12}F_{12}^{2-}$ anions. The K2 cation is located on an inversion center, and the K1 and K2 cations are rigorously coplanar. Selected interatomic distances (Å): K1−F2 and K1−F2′, 2.734(2); K1′−F3, 2.880(2); K1′−F5, 2.612(2); K2−F2, 3.324(2); K2−F3, 3.147(2); K2−F4, 2.819(2); K2−F6, 2.615(2); K1···K2, 5.543(1); K1′···K2, 5.421(1).

as shown in Table S-1.) Our DFT calculations show that the $K_2(H_2O)_n^{2+}$ dimers are thermodynamically stabilized by the lattice of anions: the ΔE values for the gas-phase dimerization of two $K(H_2O)^+$ or $K(H_2O)_2^+$ monocations into $[K(\mu\text{-}H_2O)_2K]^{2+}$ or $[(H_2O)K(\mu\text{-}H_2O)_2K(H_2O)]^{2+}$ dications are predicted to be +232 and +205 kJ mol^{-1}, respectively. The calculations also predict that ΔE for the gas-phase reaction $2\ K^+ + 2\ H_2O \rightarrow [K(\mu\text{-}H_2O)_2K]^{2+}$ is +81.0 kJ mol, whereas the enthalpy change for the reversible solid-state reaction $K_2B_{12}F_{12} + 2\ H_2O \rightarrow K_2(H_2O)_2B_{12}F_{12}$, which was measured by DSC, was found to be −111(1) kJ mol^{-1}. For comparison, the enthalpy of deposition of 2 mol $H_2O_{(s)}$ from 2 mol $H_2O_{(g)}$ is −99(1) kJ.[58]

There are significant differences in the structures of the $[K(\mu\text{-}H_2O)_2K]^{2+}$ and $[(H_2O)K(\mu\text{-}H_2O)_2K(H_2O)]^{2+}$ dications in $K_2(H_2O)_2B_{12}F_{12}$ and $K_2(H_2O)_4B_{12}F_{12}$ and their predicted gas-phase structures, as shown in Figure 6. As stated above, the K···K distances in the two hydrates range from 4.1293(5) to 4.3188(4) Å, whereas in the gas phase the predicted K···K distances are 4.886 Å for $K_2(H_2O)_2^{2+}$ and 4.835 Å for $K_2(H_2O)_4^{2+}$, ca. 0.7 Å (ca. 17%) longer. This can be understood in the following way. In the gas phase, the effective positive charge on each potassium cation is higher, and hence the repulsion between the two cations is greater than in the case of the crystalline compounds. This can be quantified to a first approximation by comparing the sums of K−O bond valences for the gas phase cations, 0.19 for $K_2(H_2O)_2^{2+}$ and 0.45 for $K_2(H_2O)_4^{2+}$, with the sums of K−O and K−F bond valences for the compounds, 1.00 for $K_2(H_2O)_2B_{12}F_{12}$ and 1.03/1.09 for $K_2(H_2O)_4B_{12}F_{12}$. In fact, the sum of K−O bond valences for $K_2(H_2O)_2B_{12}F_{12}$, 0.35, is nearly twice as large as that for the gas-phase dication $K_2(H_2O)_2^{2+}$ because, with so much more positive-charge "neutralization" in the compound, the two K^+ ions experience much less repulsion, have a much shorter K···K distance, and, as a consequence, have much shorter K−O distances.

(55) Mitani, M.; Yoshioka, Y. *THEOCHEM* **2009**, *915*, 160–169.
(56) Searles, S. K.; Kebarle, P. *Can. J. Chem.* **1969**, *47*, 2619–2627.
(57) Džidic, I.; Kebarle, P. *J. Phys. Chem.* **1970**, *74*, 1466–1474.
(58) Haynes, D. R.; Tro, N. J.; George, S. M. *J. Phys. Chem.* **1992**, *96*, 8502–8509.

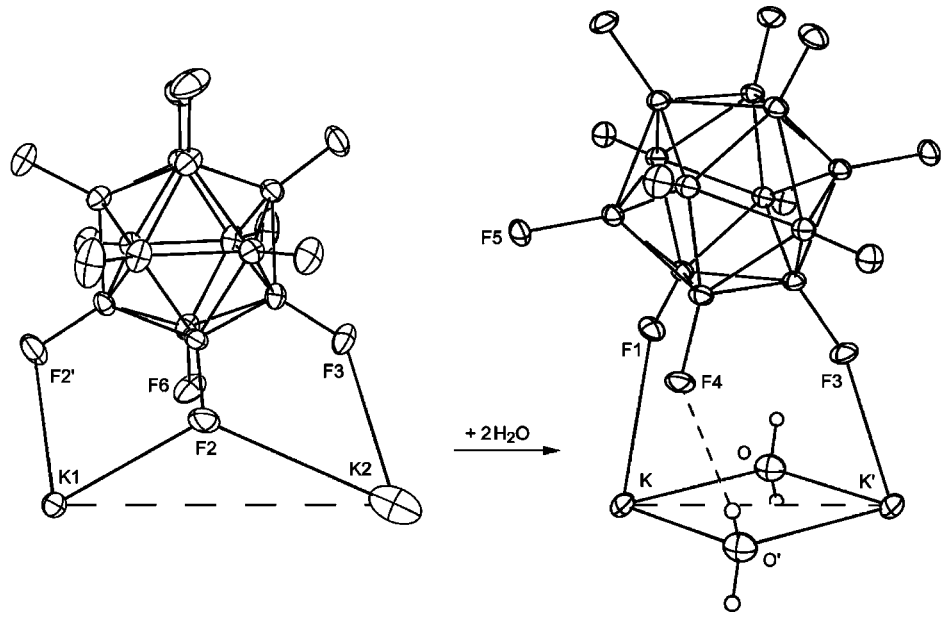

Figure 5. Parts of the structures of $K_2B_{12}F_{12}$ (left) and $K_2(H_2O)_2B_{12}F_{12}$ (right; 50% probability ellipsoids). The separation of the K^+ ions in each of the two drawings is to scale (K1′···K2 = 5.421(1) Å, K···K′ = 4.2529(3) Å). A minor rotation of pairs of $B_{12}F_{12}^{2-}$ anions (the one shown in each drawing and and its symmetry-related partner) is involved in the solid-state equilibrium $K_2B_{12}F_{12\,(s)} + 2\ H_2O_{(g)} \rightleftharpoons K_2(H_2O)_2B_{12}F_{12\,(s)}$ (F2, F2′, F3, and F6 on the left become F4, F5, F3, and F1 on the right).

The stabilization of dimeric dications by a host lattice of weakly coordinating anions was recently observed by Knapp and co-workers in $Li_2(SO_2)_8B_{12}Cl_{12}$ (a drawing of this structure is shown in Figure S-6).[59] In that case, the gas-phase dimerization of two tetrahedral $Li(SO_2)_4^+$ monocations into the observed $[(SO_2)_3Li(\mu\text{-}SO_2\text{-}1\kappa O{:}2\kappa O')_2Li(SO_2)_3]^{2+}$ dication was predicted to be endothermic by 142 kJ mol^{-1}. This is smaller than the predicted dimerization endothermicities for $[K_2(H_2O)_2]^{2+}$ (232 kJ mol^{-1}) and $[K_2(H_2O)_4]^{2+}$ (205 kJ mol^{-1}), probably for two reasons. The first reason is that the predicted Li···Li distance in the gas-phase dimer, at 5.626 Å, is ca. 0.7 Å longer than the predicted ca. 4.9 Å K···K distances (this is due to the fact that the bridging ligands in $Li_2(SO_2)_8^{2+}$ are μ-SO_2-1κO:2κO′ ligands). In fact, the predicted Li···Li distance in the gas-phase dimer is only 6% longer than the Li···Li distance in crystalline $Li_2(SO_2)_8B_{12}Cl_{12}$. The second reason is that the sums of Li−O bond valences are quite similar, 0.92 for gas-phase $Li_2(SO_2)_8^{2+}$ and 1.02 for $Li_2(SO_2)_8B_{12}Cl_{12}$. (The coordination spheres are LiO_5 in both the gas-phase dimer and in the solid-state, whereas they are KO_2 and KO_2F_6 (or KO_3 and KO_3F_5) for the potassium systems.) As points of reference, the Li···Li distances in LiF,[60] Li_2O,[61] and Li_2CrF_6[62] are 2.8475, 2.3070(5), and 2.92(2) Å, respectively.

There are 56 structures in the Cambridge Structural Database alone with $K_2(H_2O)_2$ moieties. Their refcodes are listed in Table S-2. One of them, $K_2(H_2O)_2$(*trans*-$SnMe_2F_4$),[63] is particularly relevant to the structure of $K_2(H_2O)_2B_{12}F_{12}$ because the K^+ ions in each structure are bridged only by the two H_2O molecules and because the only contacts between the cations and anions are K−F contacts. The distances and angles in the K_2O_2 core are similar to those in $K_2(H_2O)_2B_{12}F_{12}$, as shown in Figure S-7. Even the sum of K−O bond valences are the same for the two compounds, 0.35. Therefore, the water molecules are bound about as strongly in $K_2(H_2O)_2(SnMe_2F_4)$ as they are in $K_2(H_2O)_2B_{12}F_{12}$. Furthermore, the F···H(O) hydrogen bonds are also similar (1.92/1.98 Å and 161/165° in $K_2(H_2O)_2(SnMe_2F_4)$; 2.12(1)/2.17(1) Å and 154(1)/165(1)° in $K_2(H_2O)_2B_{12}F_{12}$). The biggest difference is that the coordination spheres are KO_2F_3 in $K_2(H_2O)_2(SnMe_2F_4)$, with three relatively short K−F distances of 2.60(1), 2.60(1), and 2.62(2) and K−O distances of 2.74(1) and 2.83(1) Å, and KO_2F_6 in $K_2(H_2O)_2B_{12}F_{12}$, with six K−F distances from 2.5984(4) to 3.1593(5) Å and K−O distances of 2.7698(6) and 2.7716(6) Å. The sum of K−O and K−F bond valences are 0.91 for $K_2(H_2O)_2(SnMe_2F_4)$ and, as discussed above, 1.00 for $K_2(H_2O)_2B_{12}F_{12}$. Perhaps because of the slight difference in bond-valence sums, the waters of hydration in $K_2(H_2O)_2(SnMe_2F_4)$ are not lost at room temperature, only above 50 °C, with a maximum rate of loss at 75 °C.[63] (However, the structure of $K_2(H_2O)_2(SnMe_2F_4)$ was determined at 293 K, so the bond-valence sum for K^+ would probably be somewhat higher than 0.91 at 110 K.) It is not known if the dehydration of $K_2(H_2O)_2(SnMe_2F_4)$ is reversible and, if so, if the rehydrated product is crystalline. Other relevant compounds with similar $K_2(H_2O)_2^{2+}$ cores are $K_2(H_2O)_2(Pt_2(\mu\text{-}OH)_2F_4(CF_3)_4)$ (refcode: ISITIN),[64] $K_2(H_2O)SnCl_4$,[65] $K_2(H_2O)HgCl_4$,[66] and $KF\cdot 4H_2O$.[67]

The FTIR spectrum of $K_2(H_2O)_2B_{12}F_{12}$ under ca. 21 Torr $H_2O_{(g)}$ exhibited two relatively sharp ν(OH) bands at 3638 and 3576 cm^{-1}, as shown in Figure S-8. These and relevant

(59) Knapp, C.; Schulz, C. *Chem. Commun.* **2009**, 4991–4993.
(60) Streltsov, V. A.; Tsirelson, V. G.; Ozerov, R. P.; Golovanov, O. A. *Kristallografiya* **1988**, *33*, 90–97.
(61) David, W. I. F.; Jones, M. O.; Gregory, D. H.; Jewell, C. M.; Johnson, S. R.; Walton, A.; Edwards, P. P. *J. Am. Chem. Soc.* **2007**, *129*, 1594–1601.
(62) Mazej, Z.; Goreshnik, E. *Eur. J. Inorg. Chem.* **2008**, 1795–1812.
(63) Ahmed, I. A.; Kastner, G.; Reuter, H.; Schultze, D. *J. Organomet. Chem.* **2002**, *649*, 147–151.
(64) Balters, S.; Bernhardt, E.; Willner, H.; Berends, T. *Z. Anorg. Allg. Chem.* **2004**, *630*, 257–267.
(65) Itoh, J.; Kusaka, R.; Yamagata, Y.; Kiriyama, R.; Ibamoto, H. *J. Phys. Soc. Japan* **1953**, *8*, 293–301.
(66) Aurivillius, K.; Stalhandske, C. *Acta Chem. Scand.* **1973**, *27*, 1086–1088.
(67) Beurskens, G.; Jeffrey, G. A. *J. Chem. Phys.* **1964**, *41*, 917–923.

Table 3. Calculated and Experimental Values for Potassium−Water Complexation[a]

Species or reaction	K−O Distance(s) (Å) or ΔH (kJ mol^{-1})		
	DFT, this work[b]	DFT, ref[55] [c]	exp. values[d]
$K(H_2O)^+$	2.617	2.654	
$K_2(H_2O)_2^+$	2.654	2.688	
$K_2(H_2O)_2^{2+}$	2.999[d]		
$K_2(H_2O)_4^{2+}$	2.997(b), 2.629(t)[e]		
$K^+ + H_2O \rightarrow K(H_2O)^+$	−76.3	−72.8	−75.0[f]
$K(H_2O)^+ + H_2O \rightarrow K_2(H_2O)_2^+$	−68.1	−61.5	−67.4[f]
$2K(H_2O)^+ \rightarrow K_2(H_2O)_2^{2+}$	+231.5		
$K_2(H_2O)_2^{2+} + 2H_2O \rightarrow K_2(H_2O)_4^{2+}$	−162.4		
$2K(H_2O)_2^+ \rightarrow K_2(H_2O)_4^{2+}$	+205.3		
$K_2B_{12}F_{12(s)} + 2\,H_2O_{(g)} \rightarrow K_2(H_2O)_2B_{12}F_{12(s)}$			−110(1)[g]
$2\,H_2O_{(g)} \rightarrow 2\,H_2O_{(s)}$			−99(1)[h]

[a] See Figure 6 for structures of the complexes. All reactions are in the gas phase unless otherwise noted. [b] B2PLYP-D/(aug)-def2-QZVPP. [c] B3LYP/6-31++G** with counterpoise corrected geometry optimizations. [d] High-pressure mass spectrometry; refs 56 and 57. [e] K···K = 4.886 Å. [f] K···K = 4.835 Å. [g] This work. [h] Reference 58.

frequencies for related compounds are listed in Table 4,[68−74] and the $K_2(H_2O)_2^{2+}$ moieties in $K_2(H_2O)SnCl_4$[65] and $K_2(H_2O)HgCl_4$[66] are shown in Figure S-9. The coordination of H_2O to a metal ion lowers ν(OH) values, as seen for the gas-phase $[Ar{-}K{-}OH_2]^+$ cation.[69] In addition, (O)H···X hydrogen bonding further lowers ν(OH) values and tends to broaden the bands in $K_2(H_2O)_2B_{12}F_{12}$, $K_2(H_2O)SnCl_4$,[70] $K_2(H_2O)HgCl_4$,[71] and $K_2(H_2O)_2(SnMe_2F_4)$[63] (X = F, Cl). However, the ν(OH) bands in $K_2(H_2O)_2B_{12}F_{12}$ are at higher energy and are more narrow than the bands in the other three compounds with $K_2(H_2O)_2^{2+}$ moieties, despite the fact that the K−O distances are similar in all four compounds. These results suggest that the (O)H···F hydrogen bonds in $K_2(H_2O)_2B_{12}F_{12}$ are significantly weaker than the (O)H···Cl hydrogen bonds in $K_2(H_2O)SnCl_4$ and $K_2(H_2O)HgCl_4$ or the (O)H···F hydrogen bonds in $K_2(H_2O)_2(SnMe_2F_4)$.

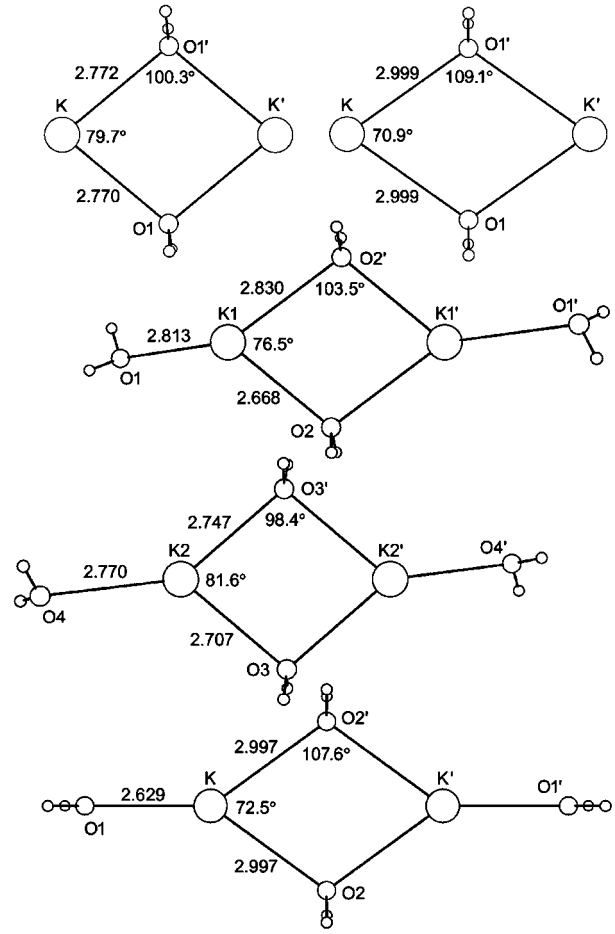

Figure 6. DFT-predicted (top right; bottom) and X-ray structures of $K_2(H_2O)_n^{2+}$ dimers. See Table 2 for the X-ray parameter standard errors.

The IR spectrum for a sample of $K_2(H_2O)_2B_{12}F_{12}$ partially exchanged with HDO and D_2O ligands is also shown in Figure S-8 (as is the IR spectrum of $K_2(H_2{}^{18}O)_2B_{12}F_{12}$). The bands assigned to HDO, which are as sharp as the bands assigned to H_2O and D_2O ligands, indicate that the two O−H bonds for each H_2O molecule are, effectively, in the same environment, even though they are not symmetry related (the (O)H1···F4 and (O)H2···F5 distances and O−H1···F4 and O−H2···F5 angles are, respectively, 2.17(1) Å, 2.12(1) Å, 154(1)°, and 165(1)°). Furthermore, the Raman spectrum of $K_2(H_2O)_2B_{12}F_{12}$ exhibited the same two ν(OH) bands as the IR spectrum (to within ±1 cm^{-1}), indicating that the vibrational coupling between the H_2O molecules in the centrosymmetric $K_2(H_2O)_2^{2+}$ cores is very weak. Finally, the A_{1g} and H_g ν(BB) Raman bands for the $B_{12}F_{12}{}^{2-}$ anion in $K_2(H_2O)_2B_{12}F_{12}$ are at 432 and 393 cm^{-1}, respectively, and these are the same values measured for a sample of the anhydrous compound $K_2B_{12}F_{12}$.

II. Dehydration/Rehydration Reactions. A. General Comments. In this section of the paper, we will describe and interpret the isothermal TGA-MS data we collected in our initial study of the reactions of the three crystalline compounds $K_2B_{12}F_{12}$, $K_2(H_2O)_2B_{12}F_{12}$, and $K_2(H_2O)_4B_{12}F_{12}$ in the presence or absence of water vapor. It is well-known that rates of solid-state reactions can depend on many factors, including the surface area and/or the surface-area-to-volume ratio of the solid particles, the partial pressures of reactive gases as they are absorbed or evolved by

(68) Herzberg, G., *Molecular Spectra and Molecular Structure II. Infrared and Raman Spectra of Polyatomic Molecules*; Kreiger: Malabar, FL, 1991.
(69) Vaden, T. D.; Weinheimer, C. J.; Lisy, J. M. *J. Chem. Phys.* **2004**, *121*, 3102–3107.
(70) Falk, M.; Huang, C.-H.; Knop, O. *Can. J. Chem.* **1974**, *52*, 2380–2388.
(71) Falk, M.; Knop, O. *Can. J. Chem.* **1977**, *55*, 1736–1744.
(72) Flaud, J. M.; Camy-Peyret, C. *J. Mol. Spectrosc.* **1974**, *51*, 142–150.
(73) Toth, R. A. *J. Opt. Soc. Am. B* **1993**, *10*, 1526–1544.
(74) Toth, R. A. *J. Mol. Spectrosc.* **1999**, *195*, 73–97.

Table 4. IR Stretching Frequencies for Water Vapor and Water Coordinated to Potassium Cations[a]

compd	K−O distance(s), Å	ν(OH) and/or ν(OD), cm^{-1}	refs[b]
$H_2O_{(g)}$	—	3756, 3657	72
$H_2{}^{18}O_{(g)}$	—	3742, 3650	73
$HDO_{(g)}$	—	3723, 2739	74
$D_2O_{(g)}$	—	2789, 2666	68
$[Ar{-}K{-}OH_2]^+_{(g)}$	—	3710, 3636[c]	69
$K_2(H_2O)_2B_{12}F_{12\,(s)}$	2.7698(6), 2.7716(6)	3638 sharp, 3576 sharp	tw
$K_2(H_2{}^{18}O)_2B_{12}F_{12\,(s)}$	—	3624 sharp, 3569 sharp	tw
$K_2(HDO)_2B_{12}F_{12\,(s)}$	—	3604 sharp, 2653 sharp	tw
$K_2(D_2O)_2B_{12}F_{12\,(s)}$	—	2700 sharp, 2616 sharp	tw
$K_2(H_2O)SnCl_{4\,(s)}$	2.650 × 2	3538 broad, 3439 broad	65, 70
$K_2(H_2O)HgCl_{4\,(s)}$	2.855(8) × 2	3505 broad, 3404 broad	66, 71
$K_2(H_2O)_2(SnF_4(CH_3)_2)_{(s)}$	2.74(1), 2.83(1)	3425 broad[d]	63

[a] All stretching frequencies are from IR spectra at room temperature unless otherwise noted; tw = this work; O = ^{16}O; sharp is defined here as $\Delta\nu_{1/2} \leq 30$ cm^{-1}; broad is defined here as $\Delta\nu_{1/2} \geq 50$ cm^{-1}. [b] The first reference is for the K−O distance(s) (if any); the second reference is for the stretching frequencies; a single reference is for both. [c] Temperature = 130 K. [d] Only one very broad band was observed.

the solid (water vapor in our case), and the temperature and/or the rate of temperature change of the sample.[75−79] For an isothermal TGA experiment, the temperature of the sample can be particularly difficult to control precisely for rapid reactions that are strongly exothermic or endothermic, which is true for the hydration and dehydration reactions studied in this work.

The mechanisms by which hydrates as simple as monohydrates are known to, or are believed to, undergo dehydration are varied, and one particular mechanism can rarely be assigned unambiguously because different mechanism functions usually fit the kinetic data equally well.[20,80−82] In fact, it may also be rare that a fixed mechanism operates throughout the entire dehydration, even for a monohydrate.[80] Dehydrations that transform one phase to another can be monovariant or, as in the case of $CaC_2O_4 \cdot H_2O$, bivariant.[81,83] With polyhydrates, of course, dehydration can occur in discrete steps or stages,[21,84] and there are examples of two-stage dehydrations that appeared to be one-step processes by TGA.[85]

All of these complications notwithstanding, we carried out an initial kinetic study of the $K_2(H_2O)_{0,2,4}B_{12}F_{12\,(s)}/H_2O_{(g)}$ system, primarily to discover whether a more in-depth kinetic study would be worthwhile in the future. For this reason, the temperature of the samples, the partial pressures of water in the TGA sample chamber during hydration/dehydration, and the sample particle sizes were known only approximately in the experiments described below. Nevertheless, some important hypotheses about the kinetics and mechanism of this equilibrium *that are supported by facts* can now be clearly stated, and experiments to test these hypotheses in the future can be intelligently designed.

B. Rapid and Irreversible Dehydration of $K_2(H_2O)_4B_{12}F_{12}$. Figure 7 shows a 25.0(5) °C TGA trace for a sample consisting of "wet" crystals of $K_2(H_2O)_4B_{12}F_{12}$, grown at 0 °C, with a thin layer of mother liquor surrounding each crystal to avoid premature dehydration (in addition, the crystals were crushed with a spatula to decrease the size of the sample particles). The carrier gas was dry helium. The ratios (molar mass $K_2(H_2O)_4B_{12}F_{12}$)/(molar mass $K_2(H_2O)_2B_{12}F_{12}$) and (molar mass $K_2B_{12}F_{12}$)/(molar mass $K_2(H_2O)_2B_{12}F_{12}$) are 1.076 and 0.924, respectively. The trace is divided into six regions labeled **a**−**f**. Region **a** is the rapid evaporation of mother-liquor water. Region **b** is the almost equally rapid dehydration of $K_2(H_2O)_4B_{12}F_{12}$ to $K_2(H_2O)_2B_{12}F_{12}$, which for this sample occured in ca. 10 min. Region **c** is the slower but still rapid dehydration of $K_2(H_2O)_2B_{12}F_{12}$ to $K_2B_{12}F_{12}$, which occured in ca. 55 min. The sample showed no further mass loss for several hours at 25.0(5) °C (region **d**), after which time the carrier gas was switched to helium bubbled through H_2O at 23(1) °C (at this temperature, $P(H_2O)$ = 21(1) Torr; note that the *sample* temperature remained 25.0(5) °C). Region **e** is the very rapid rehydration of $K_2B_{12}F_{12}$ to $K_2(H_2O)_2B_{12}F_{12}$, which occured in only 12 min for this sample. Significantly, region **f** shows that $K_2(H_2O)_2B_{12}F_{12}$ does not absorb any more water at 25.0(5) °C in the presence of 21(1) Torr $H_2O_{(g)}$, even after many hours or days (the longer times are not shown in this particular figure).

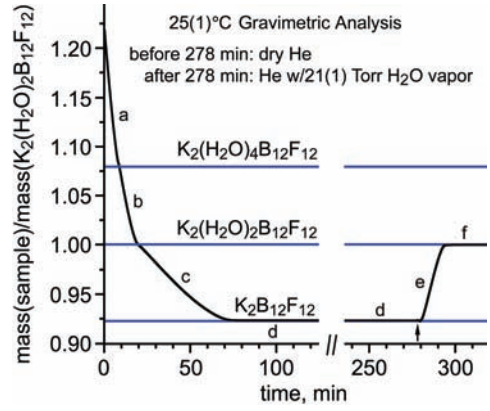

Figure 7. Constant-temperature gravimetric analysis of crushed wet crystals of $K_2(H_2O)_4B_{12}F_{12}$ at 25.0(5) °C with dry helium as the carrier gas (60 mL min^{-1}) until 278 min and helium containing 21(1) Torr $H_2O_{(g)}$ after 278 min. The horizontal lines represent the relative molar masses of the three compounds (1.076 = 507.979 g mol^{-1}; 1.000 = 471.949 g mol^{-1}; and 0.9237 = 435.918 g mol^{-1}).

Other experiments showed that $K_2(H_2O)_2B_{12}F_{12}$ does not absorb more water even when exposed to 72 Torr of $H_2O_{(g)}$ at a sample temperature of 45(1) °C. (Furthermore, $K_2(H_2O)_2B_{12}F_{12}$

(75) Vyazovkin, S.; Wight, C. A. *Annu. Rev. Phys. Chem.* **1997**, *48*, 125–149.
(76) L'vov, B. L. *Spectrochim. Acta, Part B* **1998**, *53*, 809–820.
(77) Khawam, A.; Flanagan, D. R. *Thermochim. Acta* **2005**, *429*, 92–102.
(78) Khawam, A.; Flanagan, D. R. *J. Phys. Chem. B* **2006**, *110*, 17315–17328.
(79) Galway, A. K. *J. Therm. Anal. Calorim.* **2008**, *92*, 967–983.
(80) Sheth, A. R.; Zhou, D.; Muller, F. X.; Grant, D. J. W. *J. Pharm. Sci.* **2004**, *93*, 3013–3026.
(81) Vlaev, L.; Nedelchev, N.; Gyurova, K.; Zagorcheva, M. *J. Anal. Appl. Pyrolysis* **2008**, *81*, 253–262.
(82) Boonchom, B.; Kongtaweelert, S. *J. Therm. Anal. Calorim.* **2010**, *99*, 531–538.
(83) Nerád, I.; Proks, I.; Šaušová, S. *Chem. Papers* **1991**, *45*, 721–730.
(84) Miletich, R.; Zemann, J.; Nowak, M. *Phys. Chem. Minerals* **1997**, *24*, 411–422.
(85) Paulik, F.; Paulik, J.; Arnold, M. *Thermochim. Acta* **1992**, *200*, 195–204.

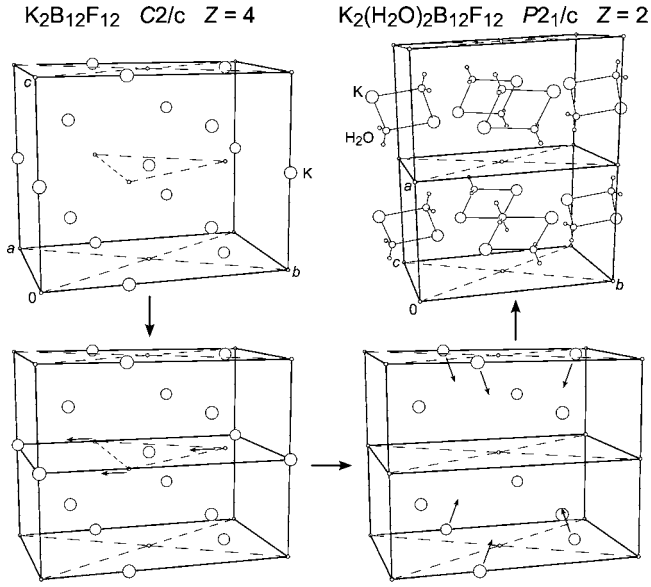

Figure 8. Relationship between the unit cell of $K_2B_{12}F_{12}$ (top left; monoclinic, $Z = 4$) and two unit cells of $K_2(H_2O)_2B_{12}F_{12}$ (top right; monoclinic, $Z = 2$), and the idealized transformation of the former into the latter by the addition of water (note that no elementary-step mechanistic detail is implied). The small circles represent the B_{12} centroids. For $K_2B_{12}F_{12}$, $a = 8.207$, $b = 14.282$, and $c = 11.344$ Å; for $K_2(H_2O)_2B_{12}F_{12}$, $2a = 14.591$, $b = 11.252$, and $c = 9.226$ Å. The 10.8% increase in unit cell volume for the reaction $K_2B_{12}F_{12\,(s)} + 2\ H_2O_{(g)} \rightarrow K_2(H_2O)_2B_{12}F_{12\,(s)}$ (i.e., 17.9 Å^3 per H_2O molecule) is largely due to an increase in the "c" axis length of ca. 1.0 Å.

is not deliquescent under these conditions.) The formation of $K_2(H_2O)_4B_{12}F_{12}$ appears to require the presence of liquid water. In this regard, the $K_2(H_2O)_{0,2,4}B_{12}F_{12}$ system resembles the $K(H_2O)_{0,2,4}F$ system (i.e., $KF\cdot(H_2O)_{0,2,4}$).[86] The KF dihydrate crystallizes from aqueous solutions in the temperature range 19−41 °C, the tetrahydrate crystallizes at lower temperatures, and anhydrous KF crystallizes at temperatures above 41.4 °C.[87] As we will discuss below, crystalline $K_2B_{12}F_{12}$ does not absorb water vapor to any extent above 52 °C.

C. Rapid, Reconstructive, and Reversible Dehydration of $K_2(H_2O)_2B_{12}F_{12}$. The observation that single crystals of $K_2(H_2O)_2B_{12}F_{12}$ were grown by the evaporation of water from a saturated aqueous solution at 25(1) °C *and* that single crystals of $K_2B_{12}F_{12}$ were grown by *very* slow evaporation of water, to dryness, of a saturated aqueous solution at 25(1) °C strongly suggests that the transformation $K_2(H_2O)_2B_{12}F_{12}(cryst) \rightarrow K_2B_{12}F_{12}(cryst) + 2\ H_2O_{(g)}$ *can* be a single-crystal-to-single-crystal transformation when it is carried out very slowly. This is sensible given the relationship between the unit cells of the two compounds, which is shown in Figure 8. Nevertheless, visual inspection of macroscopic crystals of $K_2(H_2O)_2B_{12}F_{12}$ showed that they became cloudy upon exposure to dry air (the size of the crystals used to collect the X-ray diffraction data was $0.55 \times 0.55 \times 0.28$ mm^3 for $K_2(H_2O)_2B_{12}F_{12}$ and only $0.04 \times 0.02 \times 0.01$ mm^3 for $K_2B_{12}F_{12}$). Some of the smaller cloudy single crystals were mounted on the single-crystal diffractometer and, although they were still prisms of nearly the same dimensions, gave diffraction patterns that were essentially powder rings. In addition, powder X-ray diffraction patterns of

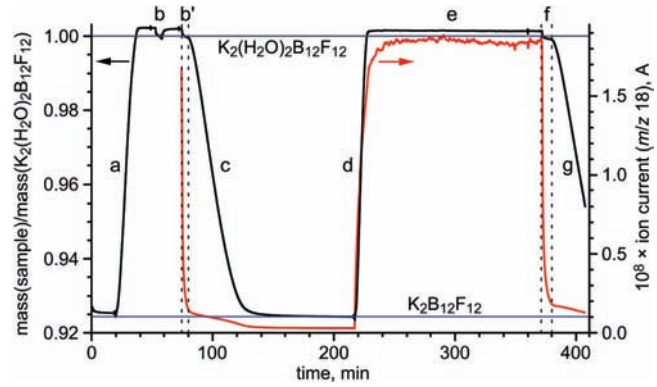

Figure 9. TGA-MS trace for two cycles of hydration/dehydration of $K_2B_{12}F_{12}$ at 25.0(5) °C. The black trace shows the relative mass of the sample; the red trace shows the mass-spectrometer response to $H_2O_{(g)}$. The carrier gas was dry helium during dehydration and helium containing 21(1) Torr $H_2O_{(g)}$ during hydration/rehydration (60 mL min^{-1}). The horizontal lines represent the relative molar masses of $K_2(H_2O)_2B_{12}F_{12}$ (1.000 = 471.949 g mol^{-1}) and $K_2B_{12}F_{12}$ (0.9237 = 435.918 g mol^{-1}).

(i) $K_2(H_2O)_2B_{12}F_{12}$ that had been formed by rehydration of crystalline $K_2B_{12}F_{12}$ in a stream of helium or nitrogen containing (nominally) 21(1) Torr of water vapor and (ii) $K_2B_{12}F_{12}$ that had been formed by dehydration of crystalline $K_2(H_2O)_2B_{12}F_{12}$ in a stream of dry helium or nitrogen indicated that both products were crystalline, as shown in Figure S-10 (the 25(1) °C experimental PXRD patterns are also compared with simulated patterns using the coordinates and symcodes for the corresponding single-crystal X-ray structures at 110(2) K). These data also indicate that the crystalline product of solid-gas hydration of crystalline $K_2B_{12}F_{12}$ at 25(1) °C is identical with that obtained by slow evaporation of an aqueous solution of the salt at 25(1) °C.

DSC experiments revealed that the dehydration of crystalline $K_2(H_2O)_2B_{12}F_{12}$ in a stream of dry nitrogen was endothermic, with $\Delta H_{298} = 111(1)$ kJ mol^{-1} (the initial temperature was 25.0(5) °C). This is only ca. 10% higher than an experimental ΔH value for $2\ H_2O_{(s)} \rightarrow 2\ H_2O_{(g)}$, which is 98.8 ± 1.6 kJ mol^{-1}.[58] Since the sample temperature in our experiments decreased to some extent during dehydration and increased during rehydration, the rates of these processes were not determined under strict isothermal conditions (a thermocouple close to the sample registered temperature changes of ±0.1 °C during the hydrations and dehydrations, and the sample temperature may have varied more than that). Two cycles of approximately constant-temperature ($T_{initial} = 25.0(5)$ °C) hydration of $K_2B_{12}F_{12}$ and dehydration of $K_2(H_2O)_2B_{12}F_{12}$ that were monitored by TGA-MS are shown in Figure 9. During the hydration cycles, the helium carrier gas was bubbled through water at 23(1) °C before entering the instrument. (Since the vapor pressure of water is 21(1) Torr at 23(1) °C,[88] we assumed that the nominal partial pressure of water in the TGA or DSC sample chamber was 21(1) Torr.) To induce dehydration, the carrier gas was switched back to dry helium. Since $K_2B_{12}F_{12}$ is known to be stable up to 550 °C,[36] the MS instrumentation was not being used to detect decomposition gases but only to monitor how quickly water vapor entered or left the sample chamber when the 23(1) °C water bubbler was included or excluded, respectively, from the carrier gas tubing (i.e., other than water

(86) Preisinger, A.; Zottl, M.; Mereiter, K.; Mikenda, W.; Steinböck, S.; Dufek, P.; Schwarz, K.; Blaha, P. *Inorg. Chem.* **1994**, *33*, 4774–4780.
(87) Magin, R. L.; Mangum, B. W.; Statler, J. A.; Thornton, D. D. *J. Res. Natl. Bur. Stand. (U.S.)* **1980**, *86*, 181–192.
(88) Lide, D. R. *Handbook of Chemistry and Physics*, 73rd ed.; CRC Press: Boca Raton, FL, 1992−1993.

vapor and small amounts of atmospheric gases, no other gases were observed).

The following observations and interpretations can be made about the black TGA trace in Figure 9 (and other results from similar experiments with samples that varied in size from 5 to 15 mg; note that the entire black trace in Figure 9 corresponds to 25.0(5) °C). First, there was almost no delay (<1 min) in the appearance of an MS ion current indicative of significant amounts of water vapor in the sample chamber after the carrier gas was switched from dry helium to helium that had been bubbled through water at 23(1) °C (compare the black and red portions of the traces for region **d** in Figure 9; the small apparent tick marks on the black trace indicate an apparent mass change when the carrier gas was changed, presumably due to a small temporary pressure change in the system; there is also an artifactual apparent temporary decrease in mass due to the introduction into the carrier gas of the small amount of higher-density air in the water-filled bubbler). Second, there was a variable delay of ca. 2−10 min before a mass decrease was observed after the carrier gas was switched back to dry helium (presumably due to relatively slow flushing of $H_2O_{(g)}$ from the sample chamber; as discussed below, dehydration only occured when $P(H_2O) \leq 7$ Torr). Third, a small amount of water adhered to the surface of the $K_2(H_2O)_2B_{12}F_{12}$ crystallites when the sample was exposed to helium containing 21(1) Torr $H_2O_{(g)}$. The amount of adsorbed water was ca. 0.014−0.030 equiv of H_2O per K^+, depending on the surface area of the sample. This would constitute, approximately, a monolayer of H_2O molecules on the surface of the crystallites if they were cubes with ca. 1 μm edges, a reasonable assumption based on SEM images shown in Figure S-11, and this amount of water disappeared rapidly when the sample was exposed to dry helium (regions **b**, **b′**, and **f**). Fourth, as discussed above, $K_2(H_2O)_2B_{12}F_{12}$ was not converted to $K_2(H_2O)_4B_{12}F_{12}$ in the presence of 21(1) Torr $H_2O_{(g)}$, even after many hours or (not shown) days. Fifth, $K_2B_{12}F_{12}$ was rapidly hydrated to $K_2(H_2O)_2B_{12}F_{12}$ in the presence of 21(1) Torr $H_2O_{(g)}$ when $T_{initial} = 25(1)$ °C, in 18 min for the hydration that began at 20 min (region **a**) and in 12 min for the hydration that began at 218 min (region **d**). Sixth, $K_2(H_2O)_2B_{12}F_{12}$ was rapidly dehydrated to $K_2B_{12}F_{12}$ in an atmosphere of dry helium when $T_{initial} = 25.0(5)$ °C, in 75 min for the dehydration that began at 75 min (region **c**) and in ca. 100 min for the dehydration that began at 218 min (region **g**; these times are for >98% dehydration).

A simple, albeit crude, kinetic figure of merit for the hydrations and dehydrations is the maximum positive or negative slopes of the TGA trace in the regions corresponding to hydration or dehydration, respectively. For example, the maximum positive slope in hydration region **d** is 1.1% min^{-1}. Note that the units of the slopes refer to the % change in mass for the complete *de*hydration process, which is 9.24%. Therefore, a maximum positive slope of 1.1% min^{-1} corresponds to an instantaneous rate of 12% of the complete hydration reaction per minute. The maximum negative slopes in dehydration regions **c** and **g** are −0.22 and −0.19% min^{-1}, respectively, the absolute values of which are ca. 5 times smaller than the hydration maximum slope of 1.1% min^{-1}.

The TGA-MS experiments showed that the rates of mass decrease and mass increase for the solid-state equilibrium $K_2(H_2O)_2B_{12}F_{12\,(s)} \rightleftharpoons K_2B_{12}F_{12\,(s)} + 2\ H_2O_{(g)}$ varied as a function of (i) sample temperature at constant $P(H_2O)$ and (ii) carrier-gas flow rate. Each of these will now be briefly discussed. A particular sample of $K_2B_{12}F_{12}$ had an average hydration maximum slope of 2.4% min^{-1} and an average dehydration maximum negative slope of −0.48% min^{-1} at 25.0(5) °C (three complete cycles). When the temperature was changed to a constant 35.0(5) °C and $P(H_2O)$ was still 21(1) Torr, the hydration maximum slope was only 0.17% min^{-1}, more than 10 times smaller than that at the lower temperature, and the dehydration maximum negative slope in the presence of dry helium was −0.96% min^{-1}, twice as large as that at the lower temperature. This is a sensible result because, at some elevated temperature, anhydrous $K_2B_{12}F_{12}$ should not absorb water even with $P(H_2O) = 21(1)$ Torr. In a subsequent nonisothermal TGA experiment, we determined that this temperature is 52 °C.

Figure S-12 shows the portion of region **d** in Figure 9 from 220 to 240 min, which represents ca. 90% of the total hydration process. It also shows that this portion of the curve could not be modeled with a single exponential function or with a sum of two exponential functions, both of which have been shown to model water sorption for microporous materials.[89] We wondered if this could be because $P(H_2O)$ was not constant throughout this portion of the curve and if the reaction rates were limited by the rate at which water vapor was delivered to the sample. To address this possibility, we carried out a series of hydrations and dehydrations of a given sample in which the carrier-gas flow rate was 30, 60, 88, or 100 mL min^{-1}. The results, shown in Figure S-13, clearly indicate that both the hydration and dehydration reactions were indeed limited by the rate at which $H_2O_{(g)}$ was delivered to or swept away from the microcrystal surfaces in these experiments. Therefore, the chemically relevant processes of (i) absorption of H_2O to $K_2B_{12}F_{12}$ unit cells at the surface of the microcrystalline sample, (ii) desorption of H_2O from $K_2(H_2O)_2B_{12}F_{12}$ unit cells at the surface of the microcrystalline sample, and (iii) the diffusion of H_2O across the constantly moving $K_2(H_2O)_2B_{12}F_{12\,(s)}$/$K_2B_{12}F_{12\,(s)}$ phase boundary *must be faster* than the fastest "hydration" and "dehydration" rates that were measured in these experiments. Note that the fastest hydration of a sample of $K_2B_{12}F_{12}$ was complete in ca. 4 min and the fastest dehydration was complete in ca. 18 min, both at the maximum carrier-gas flow rate possible with the TGA instrument used in this work.

In order to lower $P(H_2O)$ in the TGA carrier gas, helium was bubbled through various saturated aqeuous salt solutions at 23(1) °C. These experiments revealed that $K_2(H_2O)_2B_{12}F_{12}$ is not stable at 25.0(5) °C when $P(H_2O) \leq 7$ Torr (this is reported to be the vapor pressure of a saturated aqueous solution of $MgCl_2$ at ca. 23 °C;[90] we verified that it is 6(1) Torr at 23(1) °C by tensimetry). Separate tensimetric titrations of solid $K_2B_{12}F_{12}$ with water vapor showed that the equilibrium value of $P(H_2O)$ above a mixture of $K_2B_{12}F_{12\,(s)}$ and $K_2(H_2O)_2B_{12}F_{12\,(s)}$ is 6.1(3) Torr at 25(1) °C.

In a future kinetic study, lower temperatures and/or more sophisticated instrumentation will be needed to study the $K_2(H_2O)_{0,2}B_{12}F_{12\,(s)}$ system (and to study similar $[ML_n]_xB_{12}F_{12}$ solvates we have structurally characterized). At this point in time, we can only conclude that the equilibrium $K_2(H_2O)_2B_{12}F_{12\,(s)} \rightleftharpoons K_2B_{12}F_{12\,(s)} + 2\ H_2O_{(g)}$ involves, in principle, at least three elementary processes that are too fast to measure by straightforward isothermal TGA techniques at 25.0(5) °C. What sets $K_2(H_2O)_2B_{12}F_{12}$ apart from other hydrates of potassium, and perhaps from most other hydrated metal ions in the solid state at 25 °C, is that this *crystalline* dihydrate is

(89) Uchida, S.; Kawamoto, R.; Akatsuka, T.; Hikichi, S.; Mizuno, N. *Chem. Mater.* **2005**, *17*, 1367–1375, and references therein.
(90) Greenspan, L. *J. Res. Natl. Bur. Stand. A* **1977**, *81*, 89–96.

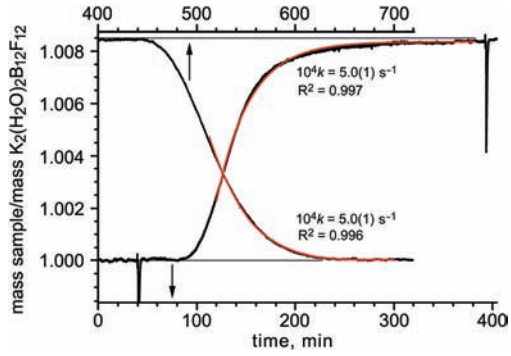

Figure 10. Gravimetric analysis for the consecutive transformations $K_2(H_2O)_2B_{12}F_{12\,(s)}$ + xs $D_2O_{(g)} \rightarrow K_2(D_2O)_2B_{12}F_{12\,(s)}$ + 2 $H_2O_{(g)}$ and $K_2(D_2O)_2B_{12}F_{12\,(s)}$ + xs $H_2O \rightarrow K_2(H_2O)_2B_{12}F_{12\,(s)}$ + 2 $D_2O_{(g)}$. The red curves are single-exponential fits to the mass (m) vs time (t) data sets covered by the red curves (i.e., the latter portion of the exchange reactions; $m \propto e^{-kt}$). The helium carrier gas was bubbled through either liquid H_2O or D_2O at 23(1) °C (the flow rate was 60 mL min^{-1}).

dehydrated extremely rapidly to the *crystalline* anhydrous salt and is even more rapidly rehydrated back to the *crystalline* dihydrate. The rapidity with which these solid-state transformations occur is especially noteworthy because $K_2B_{12}F_{12}$ is not a microporous solid (as discussed above, it has a close-packed structure[37]). To put this into perspective, the dihydrate $K_2(H_2O)_2(SnMe_2F_4)$, which has nearly the same $K_2(H_2O)_2^{2+}$ core as $K_2(H_2O)_2B_{12}F_{12}$ (see Figure S-7), undergoes dehydration between 75 and 100 °C;[63] the monohydrate $K(H_2O)MnPO_4$, in which the H_2O ligand bridges the K^+ and Mn^{2+} ions,[91] undergoes dehydration between 120 and 180 °C;[20] the monohydrate $K_2(H_2O)AlF_5$, in which the H_2O ligand bridges two K^+ ions with K−O distances of 2.818(3) and 2.821(3) Å, undergoes dehydration between 80 and 100 °C (and the anhydrous compound requires several days to rehydrate);[92] the monohydrate $K(H_2O)Zn_{2.5}V_2O_7(OH)_2$, with very long K−O distances of 3.44(2) and 3.64(4) Å, undergoes dehydration between 100 and 210 °C;[93] and a fully-dehydrated synthetic potassium gallosilicate natrolite, which is microporous, required between 1 and 2 weeks to undergo rehydration at 25 °C.[2]

D. Solid-State Diffusion of H_2O in Fully Hydrated $K_2(H_2O)_2B_{12}F_{12}$. Figure 10 shows the isothermal TGA trace for an experiment in which the carrier gas for a sample of fully hydrated $K_2(H_2O)_2B_{12}F_{12}$ at 25.0(5) °C (relative mass 1.000) was switched from helium containing 21(1) Torr $H_2O_{(g)}$ to helium containing 18(1) Torr $D_2O_{(g)}$, whereupon the sample mass increased by 0.83% (theor. 0.84% for the composition change $K_2(H_2O)_2B_{12}F_{12} \rightarrow K_2(D_2O)_2B_{12}F_{12}$), and then was switched back to helium containing 21(1) Torr $H_2O_{(g)}$, whereupon the relative sample mass returned to 1.000. Since there was a lag time between switching the carrier gas from being bubbled through liquid H_2O at 23(1) °C to being bubbled through liquid D_2O at 23(1) °C (or vice versa) and the attainment of a constant-composition atmosphere in the sample chamber, we only attempted to fit the latter one-half to two-thirds of the relevant portions of the mass (m) vs time (t) TGA trace to the single exponential equation $m \propto e^{-kt}$. Both fits resulted in the same value of the time constant $10^3k = 0.50\ s^{-1}$.

A different sample, presumably with a different average particle size, resulted in exponential fits with a different value of $10^3k = 1.9\ s^{-1}$, which was also the same whether H_2O replaced D_2O in the solid sample or vice versa, as shown in Figure S-14, and the isotopomer exchange was complete in less than 1 h at 25.0(5) °C. Furthermore, $10^3k = 1.9\ s^{-1}$ whether $P(H_2O)$ was 21(1) Torr or 16(1) Torr, as also shown in Figure S-14. These results strongly suggest that the measured rate is the rate of H_2O diffusion within fully hydrated $K_2(H_2O)_2B_{12}F_{12}$, although the "fully hydrated" compound may contain a small percentage of water-vacancy defects.

We have not attempted to calculate a diffusion coefficient for the waters of hydration in $K_2(H_2O)_2B_{12}F_{12}$ in order to compare it to literature values for other compounds because we would have to assume a particular model for diffusion and the sample would have to have a known, uniform particle size and particle morphology. Instead we intend to measure the diffusion coefficient by solid-state NMR techniques in the near future. However, at the present time the following qualitative comparisons can be made. The mineral lawsonite, $CaAl_2Si_2O_7(OH)_2 \cdot H_2O$, was reported to undergo H_2O/D_2O and OH/OD exchange in the presence of 24 Torr $D_2O_{(g)}$ at 382 °C in ca. 150 h;[1] the four lattice H_2O molecules in a 4.6 mg single crystal of $UO_2(NO_3)(H_2O)_2 \cdot 4H_2O$ were reported to undergo H_2O/D_2O exchange in ca. 36 min at 25 °C (but the two coordinated H_2O ligands did not undergo exchange to any extent under these conditions);[94] and the exchange of all 12 H_2O molecules in microcrystalline β-cyclodextrin dodecahydrate with either $D_2O_{(g)}$ or $H_2{}^{18}O_{(g)}$ at 25 °C was 90+% complete after ca. 1 h or longer depending on particle size.[13,95] To provide an additional example, we measured the initial rate of exchange of $D_2O_{(g)}$ with microcrystalline $CuSO_4 \cdot 5H_2O$ and found that only 0.15 equiv of D_2O had exchanged with the five waters of hydration after 2 h at 25.0(5) °C.

III. Concept of Latent Porosity. The facile dehydration and rehydration, and H_2O/D_2O or $H_2O/H_2{}^{18}O$ exchange, of $K_2(H_2O)_2B_{12}F_{12}$ at 25 °C suggests that microporosity is not a requirement for rapid diffusion of reactive gases in solids. The close-packed structure of crystalline $K_2B_{12}F_{12}$ shows that it has no empty spaces, let alone channels, the size of H_2O molecules[37] (this was determined using the program PLATON[96]). We have now shown that this lattice can increase in volume by 10.8%, accomodating two H_2O molecules, in 4 min or less at 25 °C. This is an example of "virtual" or "latent" porosity, the rapid creation of space to accomodate reactive gases on demand. This concept is related to, but distinct from, recent work on solids that are already microporous but that require flexible lattices to open existing pores so that they are accessible to gas molecules, as in the recent elegant study by Shimizu and co-workers.[21] In that work, involving Ba^{2+} cations and organosulfonate anions, the dehydrated phase is stable at 550 °C (like $K_2B_{12}F_{12}$) and the facile opening and closing of pore spaces is believed to be a function of "the diffuse ionic nature of the intermolecular interactions and the adaptable coordination preferences of

(91) Carling, S. G.; Day, P.; Visser, D. *Inorg. Chem.* **1995**, *34*, 3917–3927.
(92) de Kozak, A.; Gredin, P.; Pierrard, A.; Renaudin, J. *J. Fluorine Chem.* **1996**, *77*, 39–44.
(93) Hoyos, D.; Paillaud, J.-L.; Simon-Masseron, A.; Guth, J.-L. *Solid State Sci.* **2005**, *7*, 616–621.
(94) Franklin, M. L.; Flanagan, T. B. *J. Phys. Chem.* **1971**, *75*, 1272–1278.
(95) Moreira da Silva, A. M.; Steiner, T.; Saenger, W.; Empis, J.; Teixeira-Dias, J. J. C. *Chem. Commun.* **1997**, 465–466.
(96) Spek, A. L. *Acta Crystallogr.* **2009**, *D65*, 148–155.

both metal and ligand components."[21] Compounds containing metal ions from throughout the periodic table and the large, highly symmetric, robust, and superweak fluoroanion $B_{12}F_{12}^{2-}$ may provide a new class of reactive solids with latent porosity, and we are currently pursuing that possibility.

Acknowledgment. We thank Travis C. Folsom and D. Luke Heyliger for performing the vacuum-line tensimetry experiments; Dr. Zoran Mazej for obtaining the Raman spectrum of anhydrous $K_2B_{12}F_{12}$; Dr. Patrick R. McCurdy for obtaining the SEMs of $K_2B_{12}F_{12}$; Professors John R. Ridley, Amy L. Prieto, Paul Kebarle, and Steven M. George for helpful discussions; and Professor Dr. Lothar Dunsch for his continuing support. This work was supported by the Colorado State University Foundation, ERC, Inc., and Edwards AFB, CA (AFRL-RZSP).

Supporting Information Available: Crystallographic information files for $K_2(H_2O)_2B_{12}F_{12}$ and $K_2(H_2O)_4B_{12}F_{12}$ and additional figures and tables. This material is available free of charge via the Internet at http://pubs.acs.org.

Note Added in Proof. A recent paper reviews some of the problems with attempts to draw chemical insight from solid-state kinetics: Finney, E. E.; Finke, R. G. *Chem. Mater*. **2009**, *21*, 4692−4705.

JA105522D